NACA

RESEARCH MEMORANDUM

CHARTS FOR DETERMINING PRELIMINARY VALUES OF SPAN-LOAD, SHEAR, BENDING-MOMENT, AND ACCUMULATED-TORQUE DISTRIBUTIONS OF SWEPT WINGS OF VARIOUS TAPER RATIOS

By

Bertram C. Wollner

Langley Aeronautical Laboratory
Langley Field, Va.

NATIONAL ADVISORY COMMITTEE
FOR AERONAUTICS

WASHINGTON

July 6, 1948

NACA RM No. L8A26

NATIONAL ADVISORY COMMITTEE FOR AERONAUTICS

RESEARCH MEMORANDUM

CHARTS FOR DETERMINING PRELIMINARY VALUES OF SPAN-LOAD, SHEAR, BENDING-MOMENT, AND ACCUMULATED-TORQUE DISTRIBUTIONS OF SWEPT WINGS OF VARIOUS TAPER RATIOS

By Bertram C. Wollner

SUMMARY

Charts are presented which may be used in determining preliminary values of the spanwise-load, shear, bending-moment, and the accumulated-torque distributions of swept wings of various taper ratios. The charts are based on strip theory and include four aerodynamic-load distributions, two section-moment distributions, and two inertia-load distributions. The taper ratios considered cover the range from 1.0 to 0, and the results are applicable to any angle of sweep. The curves are useful in preliminary design work where only a rough idea of the magnitudes of shear and bending moment is required.

In order to illustrate the accuracy of the present results, some comparisons with results calculated by more accurate methods are given of the loads, shears, and bending moments for a hypothetical airplane operating at different speed ranges.

An example is also included to illustrate the use of the charts and to show typical results.

INTRODUCTION

Since the determination of the load distribution over a swept wing, even in the subsonic range where incompressible fluid is assumed, may be a long and tedious process, the fact that load distributions for several speed ranges may be required makes it desirable that some quick and easy method be available by which preliminary results may be determined.

For this reason, strip theory has been used to establish a series of nondimensional charts by which the load, shear, bending moment, and accumulated torque at any point along the wing span may readily be determined. The charts, together with the specification of load factors, angular velocity, and angular acceleration to be used, should serve as a preliminary guide in determining the sizes of the structural elements required to support the load. The results are given in as general a form

as possible and consist of charts covering the distributions due to the additional air load, air loads due to an equal and opposite aileron deflection, built-in-twist, damping-in-roll, wing-weight, normal-inertia, and angular-inertia distributions. The torques about the elastic axis, parallel to the X-Z plane, due to the section pitching moments as well as those due to the above-mentioned air and inertia-load distributions are also included. The charts cover the range of taper ratios from the rectangular to the pointed wing.

SYMBOLS AND SIGN CONVENTIONS

n	wing load factor
W	gross airplane weight, pounds
W_w	wing weight, pounds
b	wing span, feet
b_a	aileron span, feet
c	wing chord at any station, feet
$\bar{c}$	average chord of wing, feet
y	lateral distance measured from plane of symmetry, feet
k	lateral distance measured from plane of symmetry as fraction of semispan $\left(\frac{y}{b/2}\right)$
k_1	distance from leading edge to line of aerodynamic centers as a fraction of the chord
k_2	distance from leading edge to elastic axis as a fraction of the chord
k_3	distance from leading edge to line of section center of gravity as a fraction of the chord
α	angle of attack, degrees
δ	aileron angle measured in plane parallel to plane of symmetry, radians; positive downward
ϵ	angle of built-in twist from root to tip, radians; washin positive

C_{L_α}	rate of change of wing lift coefficient with angle of attack, per radian
c_{l_α}	effective section lift slope; rate of change of wing-section lift coefficient with wing angle of attack, per radian
c_{l_δ}	rate of change of wing-section lift coefficient with aileron deflection, per radian
α_δ	rate of change of wing-section angle of attack with aileron deflection for constant lift at section $\left(\frac{c_{l_\delta}}{c_{l_\alpha}}\right)$
λ	wing taper ratio
q	dynamic pressure, pounds per square foot
V	true airspeed, feet per second
M	Mach number
Λ	angle of sweep measured from the Y-axis to the line of aerodynamic centers, degrees; sweepback positive
p	angular velocity in roll, radians per second
$\dot{p}$	angular acceleration in roll, radians per second per second
pb/2V	helix angle described by wing tip, radians
g	gravitational constant, feet per second per second
c_{m_o}	wing-section pitching-moment coefficient about its aerodynamic center
Δc_m	increment in wing-section pitching-moment coefficient about its aerodynamic center due to aileron deflection
l	running load at any spanwise station, pounds per foot
Q	vertical shear at any spanwise station, pounds
BM	vertical bending moment at any spanwise station, foot-pounds
T	accumulated torque at any spanwise station, pound-feet

In addition to the preceding symbols, the following sign conventions are used:

1. Upward-acting loads on the wing, whatever the source, and their resulting shears and bending moments are considered positive. Thus, in connection with the air loads on the wing due to angular velocity in roll and the inertia loads due to angular acceleration, the signs may be either positive or negative, depending on the wing being considered and the direction of the roll.

2. Pitching moments tending to stall the airplane are considered positive.

Other sign conventions followed in this report are shown in figure 1.

BASIS OF CHARTS

Geometric Characteristics of Wings

The charts given in this report strictly apply to tapered wings having the following geometric characteristics:

1. The slopes of the leading and trailing edges are constant along the span.

2. The lines of aerodynamic centers, elastic centers, and centers of gravity of the sections are straight and are located at constant fractions of the chord behind the leading edge.

3. Ailerons and flaps have constant flap-chord ratios along the span and hence introduce constant values of Δc_m.

4. Any built-in or aerodynamic twist varies linearly along the span.

5. The wing section and hence the pitching-moment coefficient is constant along the span.

Assumptions

In addition to the above geometric restrictions, the following assumptions were made:

1. The magnitude of the normal-force component at a given spanwise station is proportional to the chord and the angle of attack at the station.

2. The magnitude of the wing dead weight at any spanwise station is proportional to the chord.

The forces and moments considered act along the lines and planes shown in figure 1. Loads and shears are given in planes parallel to the X–Z plane. Bending moments and torques are calculated about axes parallel to the X–axis and Y–axis, respectively.

LOAD DISTRIBUTIONS

The load distributions covered by the charts consist of the four aerodynamic and two inertia or dead–weight loadings shown in figures 2 and 3, respectively. These figures also show the methods for obtaining numerical results from the charts given in figures 4 to 12. The accumulated–torque distributions are shown so that the effects upon the components of the total torque distribution of the displacement of the elastic axis from the aerodynamic centers of sweep, and of the displacement of the section centers of gravity from the aerodynamics centers may be seen.

Additional–load distribution.– This is the distribution associated with a rigid, untwisted wing, and under the assumptions made it is constant in shape and varies with the load factor. The nondimensional loads, shears, bending moments, and torques due to this distribution are given in figures 4, 9(a), and 9(b). In order to obtain the actual values of load, shear, bending moment, and torque in a given case, the numerical value of the ordinate at any spanwise station is multiplied by the numerical value of the factor given in figure 2 which may be determined from the conditions of the problem.

Ailerons–deflected distribution.– The load distribution due to deflecting the ailerons equally and oppositely is a zero lift distribution and does not affect the total lift. The load depends on the amount of aileron deflection as well as on the aileron effectiveness and dynamic pressure. The nondimensional loads, shears, bending moments, and torques due to this distribution are given in figures 4, 5, 9(a), 9(b), and 10. The load distributions shown apply only over the part of the span containing the aileron, the load becoming zero at the inboard end of the aileron. The shear becomes constant inboard of the control surface. The bending–moment and torque distributions given apply to ailerons of various span ratios as noted on the figures. Actual values of the load, shear, bending moment, and torque are obtained as before.

Built–in–twist distribution.– A linear built–in twist in the wing will cause distributions as shown in figures 6 and 11. In computing the distributions due to built–in twist alone, it is necessary to subtract an additional load equal to the load caused by the twist to obtain a zero lift distribution. The resulting distribution varies with angle of twist and dynamic pressure. Numerical values of the load, shear, bending moment, and torque in a given case are obtained as shown in figure 2.

Damping-in-roll distribution.- The rolling velocity caused by the equal and opposite aileron deflection results in a damping moment. The load distribution due to this damping moment is computed as though the wing has a linear antisymmetrical twist increasing from zero at the airplane center line to a value of the wing-tip helix angle $pb/2V$ at the tip. This distribution is dependent upon the wing-tip helix angle and the dynamic pressure. The distributions due to damping in roll are given in figures 7, 12(a), and 12(b).

Section pitching-moment distribution.- The torque distribution is caused by the pitching-moment coefficients of the sections. Under the assumptions made previously in this report the wing sections and consequently the section pitching-moment coefficients are constant along the span of the wing. The distribution varies as the dynamic pressure and is shown in figure 8.

Deflecting the ailerons equally and oppositely causes a change in the pitching-moment coefficient. This increment will be constant along the aileron span since the aileron chord - wing chord ratio is assumed constant. The distribution varies as the dynamic pressure. The results shown in figure 8 apply over the aileron span. Inboard of the aileron the accumulated torque due to this increment remains constant.

Wing-weight and normal-inertia distribution.- This distribution results from the structural weight of the wing. Under the assumption made it is proportional to the chord and varies with the load factor and wing weight. The results applicable to this distribution are given in figures 4 and 9. The ordinates of the figures are used in conjunction with the factors given in figure 3 to obtain numerical values of load, shear, bending moment, and accumulated torque.

Angular-inertia distribution.- Angular acceleration in roll produces an angular-inertia distribution which varies as the angular rolling acceleration. This distribution is assumed to be proportional to the chord and the relative distance along the span. Figures 7 and 12 present the load, shear, bending-moment, and accumulated-torque distributions applicable to this loading. Numerical values are obtained as explained in figure 3.

APPLICATION OF CHARTS

In order to apply the charts, numerical values of the quantities listed in table I are required. Many of these will be determined from the geometric characteristics of the airplane while others will depend upon the design conditions to be investigated. The angle δ and the aerodynamic quantities a_δ and c_{l_α} to be used call for additional comment, however, if reasonably accurate magnitudes of the load distributions directly affected by them are to be obtained.

As defined in the symbols, δ is measured parallel to the plane of symmetry.

The value of α_δ to be used should be applicable to the particular section geometry of the aileron to be used and should be corrected for any Mach number or other effects that may exist. A guide to the value of α_δ may be obtained from various NACA data reports.

The value of the effective slope c_{l_α} to be used is more difficult to determine, being influenced by both Mach number and sweep and being neglected in the derivation of the charts. Since induction effects were neglected, it would be expected that errors on this account would be lowest where such effects are a minimum, that is, at large aspect ratios. Unfortunately, low aspect ratio and sweep usually occur together so that to obtain a practical value of c_{l_α} it is suggested that the lift-curve slope for the entire wing C_{L_α} be substituted for the section lift slope c_{l_α}. The lift-curve slope for the finite wing C_{L_α} could then be obtained either from tests of a wing of geometrically similar plan form or, lacking such data, from the relation

$$C_{L_\alpha} = \frac{(A + 2) \cos \Lambda}{A + 2 \cos \Lambda} C_{L_{\alpha_{\Lambda=0}}}$$

where the slope for zero sweep angle $C_{L_{\alpha_{\Lambda=0}}}$ is appropriate to the Mach number in question. The above equation takes both sweep and first-order induction effects into account and is based on an unpublished analysis from the Langley stability tunnel.

For best results the charts presented in this report should be used only to determine critical wing loads.

To illustrate the use of the charts, the loads on the right wing will be determined for a hypothetical airplane with swept wings in an abrupt rolling pull-out to the right. This maneuver is chosen because it illustrates the use of the figures and indicates the relative importance of the various distributions. Values of the characteristics of a typical high-speed airplane with sweptback wings are assumed and are shown in table I.

Typical Calculation at 40-Percent-Semispan Station

Additional air load = $F_1\frac{nW}{b}$ (fig. 2)

F_1 at station 40 = 1.06 (fig. 4)

$\frac{nW}{b}$ = 4000 (table I)

Load = 1.06 × 4000 = 4240 lb/ft

Ailerons-deflected load = $F_1 c_{l_\alpha} \alpha_\delta \delta q \bar{c}$ (fig. 2)

F_1 at station 40 = 0 as this station is inboard of the aileron

Load = 0

Built-in-twist load = $F_4 c_{l_\alpha} \epsilon q \bar{c}$ (fig. 2)

F_4 at station 40 = −0.05 (fig. 6)

$c_{l_\alpha} \epsilon q \bar{c}$ = 335.1 (table I)

Load = −0.05 × 335.1 = −17 lb/ft

Damping-in-roll load = $F_7 c_{l_\alpha} \frac{pb}{2V} q \bar{c}$ (fig. 2)

F_7 at station 40 = 0.43 (fig. 7)

$c_{l_\alpha} \frac{pb}{2V} q \bar{c}$ = 768 (table I)

Load = 0.43 × 768 = 330 lb/ft

Wing weight and normal load = $F_1\frac{nW_w}{b}$ (fig. 3)

F_1 at station 40 = 1.06 (fig. 4)

$\frac{nW_w}{b}$ = 750 (table I)

Load = −1.06 × 750 = −795 lb/ft

Angular-inertia load = $F_7 \frac{\dot{p}}{g} \frac{W_w}{2}$ (fig. 3)

F_7 at station 40 = 0.43 (fig. 7)

$\frac{\dot{p}}{g} \frac{W_w}{2}$ = 163.5 (table I)

Load = −0.43 × 163.5 = −70 lb/ft

The total load at the 40-percent-semispan station is the sum of the increments, 3688 pounds per foot.

The distribution of shear, bending moment, and accumulated torque along the span was found in a similar manner through the use of the curves of figures 4 to 12 and the factors given in table I.

The loadings were determined along the semispan of the right wing. The load, shear, bending moment, and accumulated torque are shown in figures 13, 14, 15, and 16, respectively. In the figures each increment is plotted separately to show the relative importance of each component of the total distributions.

DISCUSSION

For simplicity in manufacture, many swept wings are designed with the chordwise members perpendicular to some constant percent chord line. Moments in planes parallel and perpendicular to the chordwise members are usually considered in determining the necessary structure for such a design. The results obtained from the charts, which apply to sections parallel to the relative wind, may be adapted to this type of wing structure by adding the components of the bending moment and torque acting in this direction at the station under consideration. This will result in a new torque given by

$$T' = BM \sin \Lambda' + T \cos \Lambda'$$

and a new bending moment

$$BM' = BM \cos \Lambda' - T \sin \Lambda'$$

where Λ' is the angle of sweep of the selected datum.

Although the charts are derived for loads which are considered distributed, large concentrated weights such as landing gear, machine guns, ammunition, and so forth, that may be housed in the wing may easily be taken into account.

The charts are applicable to wings of plan forms other than trapezoidal. So that distributions equivalent to those of the original wing may be obtained, a trapezoidal wing with area and centroid equal to those of the original wing should be used. If the center of area of the original wing $\bar{k}$ is known, the taper ratio of the equivalent trapezoidal wing may be found from the relation

$$\lambda = \frac{3\bar{k} - 1}{2 - 3\bar{k}}$$

The dimensions of the trapezoidal wing may now be determined, area and taper ratio being known. An example of this modification is shown in figure 17 which also shows the effects of such a substitution upon the accuracy of the distributions due to the additional air load. The distributions shown for the elliptical wing were obtained from reference 1. Other variable factors such as built-in or aerodynamic twist are assumed linear, whereas flap-chord ratio, positions of the lines of centers, and wing section are assumed constant. Although the use of the charts in this manner may reduce the accuracy of the results obtained, they should still be suitable for preliminary design work, provided the departure from the original wing is not too great.

It may be seen from the results of the typical example as shown in figures 13 to 16 that the largest part of the total distributions is due to the additional air load. The next largest part is caused by wing weight and normal inertia. The loads due to damping in roll and to an equal and opposite aileron deflection account for smaller parts of the total distributions while angular inertia and built-in twist account for even smaller parts. In the case of the torques, that due to the additional load is considerably larger than that due to the section pitching moment because of the small value of c_{m_o} selected. In a straight wing this is almost never the case because the additional load usually introduces only small torque values about the elastic axis as compared with that due to section pitching moment, which is independent of sweep. The introduction of sweep, however, results in an increase of the torque value due to the additional air load above that due to section pitching moment. Since the additional load curve is automatically adjusted to obtain the area under the load curve corresponding to the assigned load factor, good accuracy can be expected. The load components due to built-in twist, damping in roll, and ailerons deflected will probably not be known to the same degree of accuracy, on a percentage basis. However, since these components present relatively small contributions at the critical load condition, the lack of accuracy could be tolerated in preliminary design work.

In order to indicate the relative accuracy of the results obtained from the charts with results from more accurate methods and with experiment, several comparisons are shown in figures 18 to 20. These comparisons are made for equal total lift on the wings, that is, equal shears at the wing root. They are made for a wing with taper ratio of 0.418 since this was the only ratio for which applicable experimental data were available. The other characteristics remain as shown in table I. Curves 1 in the figures represent the distributions due to the additional air load obtained from the charts. The experimental subsonic distributions are given by curves 2 and are based on data from work done at Ames Aeronautical Laboratory by N. H. Van Dorn and John DeYoung. The corresponding theoretical distributions from Falkner's method (reference 2) are given as curves 3. The supersonic distributions given by figures 21 to 23 were computed using the method of reference 3 for $M = 1.414$. It may be seen that since the results from the charts show these results to be at the most 15 percent

low (in the supersonic case), the charts are of sufficient accuracy to be used in preliminary design work. However, it should be noted that somewhat poorer agreement may be expected at higher Mach numbers depending on the configuration of the design.

CONCLUDING REMARKS

Charts have been presented for use in determining preliminary values of spanwise-load, shear, bending-moment, and accumulated-torque distributions of swept wings of various taper ratios.

The charts will give results that are reasonably accurate when compared with distributions determined by means of more accurate and laborious methods. On the basis of these results, the charts may be considered as being applicable in preliminary design work.

Langley Memorial Aeronautical Laboratory
National Advisory Committee for Aeronautics
Langley Field, Va.

REFERENCES

1. Pearson, Henry A., and Aiken, William S., Jr.: Analysis of Effect of Rolling Pull-Outs on Wing and Aileron Loads of a Fighter Airplane. NACA ARR No. L5I04, 1946.

2. Falkner, V. M.: The Calculation of Aerodynamic Loading on Surfaces of Any Shape. R. & M. No. 1910, British A.R.C., 1943.

3. Brown, Clinton E.: Theoretical Lift and Drag of Thin Triangular Wings at Supersonic Speeds. NACA TN No. 1183, 1946.

TABLE I

VALUES ASSUMED FOR EXAMPLE

Load factor, n	8.0
Gross airplane weight, W, lb	16,000
Wing weight, W_w, lb	3000
Wing span, b, ft	32
Average wing chord, $\bar{c}$, ft	8
Wing taper ratio, λ	0.50
Sweepback, Λ, deg	45
Aileron span ratio, b_a/b	0.50
Aileron chord ratio, c_a/c	0.25
Chordwise location of aerodynamic centers, k_1	0.25
Chordwise location of elastic centers, k_2	0.45
Chordwise location of centers of gravity, k_3	0.50
Angle of built-in twist of wing, ϵ, deg	1.0
Slope of section lift curve, c_{l_α}, per radian	6.0
Aileron effectiveness factor, α_δ, deg	0.50
Pitching-moment coefficient, c_{m_o}	-0.01
Increment in pitching-moment coefficient, Δc_m	0.03
Dynamic pressure, q, lb/sq ft	400
Aileron angle, δ, deg	-3.0
Wing-tip helix angle, pb/2V, radian	0.04
Angular acceleration in roll, $\dot{p}$, radian/sec/sec	3.5

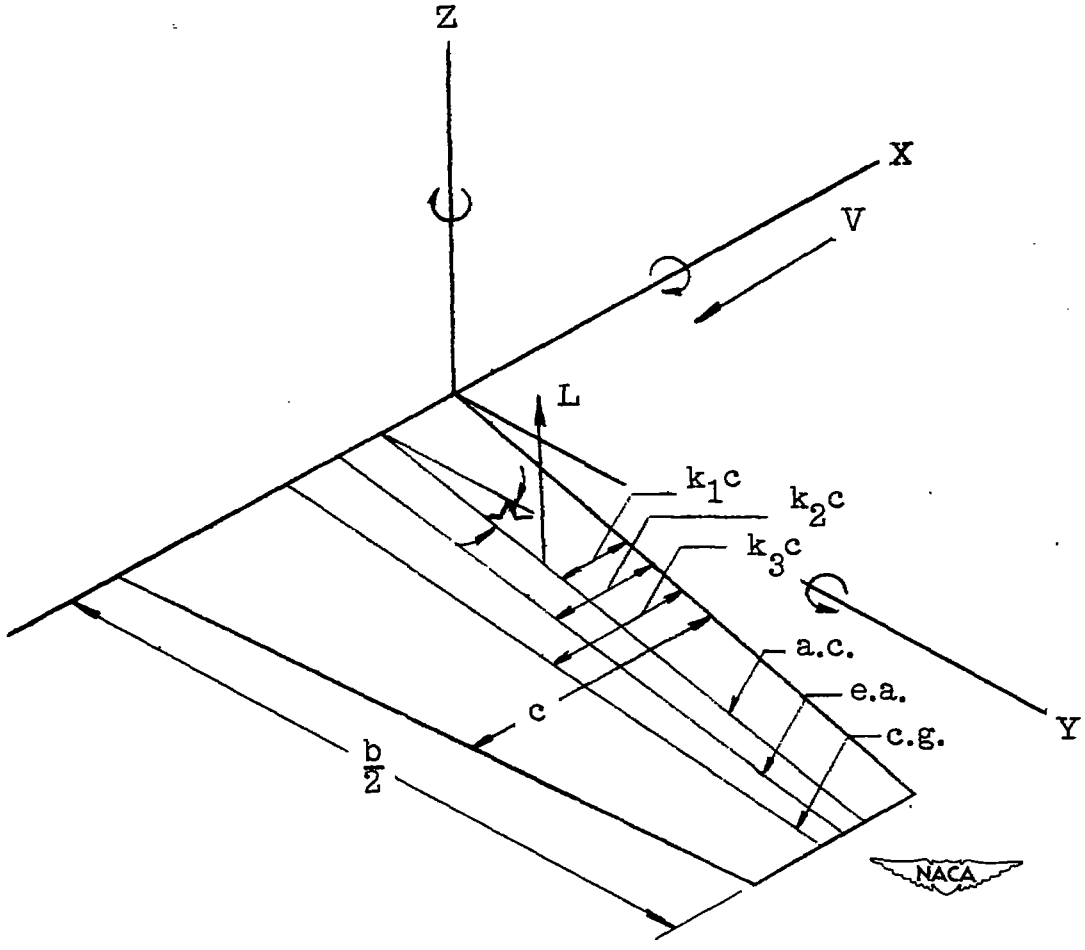

Figure 1.- Sign conventions employed. Positive directions and dimensions are shown.

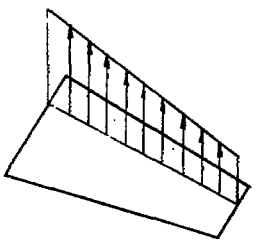

Additional Load Distribution

Load, lb/ft

$$F_1 \times nW/b$$

Shear, lb

$$F_2 \times nW$$

Bending Moment, ft-lb

$$F_3 \times nWb$$

Accumulated Torque, lb-ft

$$F_{11} \times nW\bar{c}\,(k_2 - k_1) + F_{12} \times nWb \tan \Lambda$$

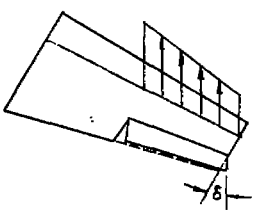

Ailerons-deflected Distribution

Load, lb/ft

$$F_1 \times c_{l_a} a_\delta \delta q \bar{c}$$

Shear, lb

$$F_2 \times c_{l_a} a_\delta \delta q b \bar{c}$$

Bending Moment, ft-lb

$$F_3 \times c_{l_a} a_\delta \delta q b^2 \bar{c}$$

Accumulated Torque, lb-ft

$$F_{11} \times c_{l_a} a_\delta \delta q b \bar{c}^2 (k_2 - k_1) + F_{12} \times c_{l_a} a_\delta \delta q b^2 \bar{c} \tan \Lambda$$

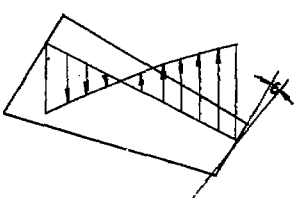

Built-in Twist Distribution

Load, lb/ft

$$F_4 \times c_{l_a} \epsilon q \bar{c}$$

Shear, lb

$$F_5 \times c_{l_a} \epsilon q b \bar{c}$$

Bending Moment

$$F_6 \times c_{l_a} \epsilon q b^2 \bar{c}$$

Accumulated Torque, lb-ft

$$F_{14} \times c_{l_a} \epsilon q b \bar{c}^2 (k_2 - k_1) + F_{15} \times c_{l_a} \epsilon q b^2 \bar{c} \tan \Lambda$$

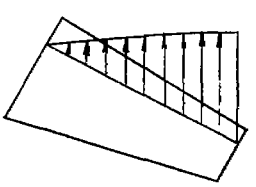

Damping-in-roll Distribution

Load, lb/ft

$$F_7 \times c_{l_a} \frac{pb}{2V} q \bar{c}$$

Shear, lb

$$F_8 \times c_{l_a} \frac{pb}{2V} q b \bar{c}$$

Bending Moment, ft-lb

$$F_9 \times c_{l_a} \frac{pb}{2V} q b^2 \bar{c}$$

Accumulated Torque, lb-ft

$$F_{16} \times c_{l_a} \frac{pb}{2V} q b \bar{c}^2 (k_2 - k_1) + F_{17} \times c_{l_a} \frac{pb}{2V} q b^2 \bar{c} \tan \Lambda$$

Section Pitching Moment Distribution

Accumulated Torque, lb-ft

$$F_{10} \times c_{m_o} q b \bar{c}^2$$

Increment in Section Pitching Moment Distribution Caused by Aileron Deflection

Accumulated Torque, lb-ft

$$F_{10} \times \Delta c_m q b \bar{c}^2$$

Figure 2.- Summary of aerodynamic load distributions considered.

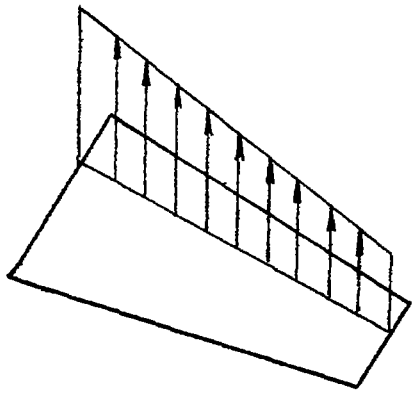

Wing Weight and Normal Inertia Distribution

Load, lb/ft

$$F_1 \times nW_w/b$$

Shear, lb

$$F_2 \times nW_w$$

Bending Moment, ft-lb

$$F_3 \times nW_w b$$

Accumulated Torque, lb-ft

$$F_{11} \times nW_w\bar{c}\,(k_2 - k_1) + F_{12} \times nW_w b \tan \Lambda + F_{13} \times nW_w\bar{c}\,(k_3 - k_1)$$

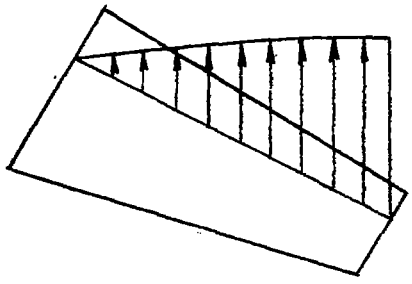

Angular Inertia Distribution

Load, lb/ft

$$F_7 \times \frac{\dot{p}}{g}\frac{W_w}{2}$$

Shear, lb

$$F_8 \times \frac{\dot{p}}{g}\frac{W_w b}{2}$$

Bending Moment, ft-lb

$$F_9 \times \frac{\dot{p}}{g}\frac{W_w b^2}{2}$$

Accumulated Torque, lb-ft

$$F_{16} \times \frac{\dot{p}}{g}\frac{W_w}{2} b\bar{c}\,(k_2 - k_1) + F_{17} \times \frac{\dot{p}}{g}\frac{W_w}{2} b^2 \tan \Lambda + F_{18} \times \frac{\dot{p}}{g}\frac{W_w}{2} b\bar{c}\,(k_3 - k_1)$$

Figure 3.- Summary of Inertia Distributions Considered.

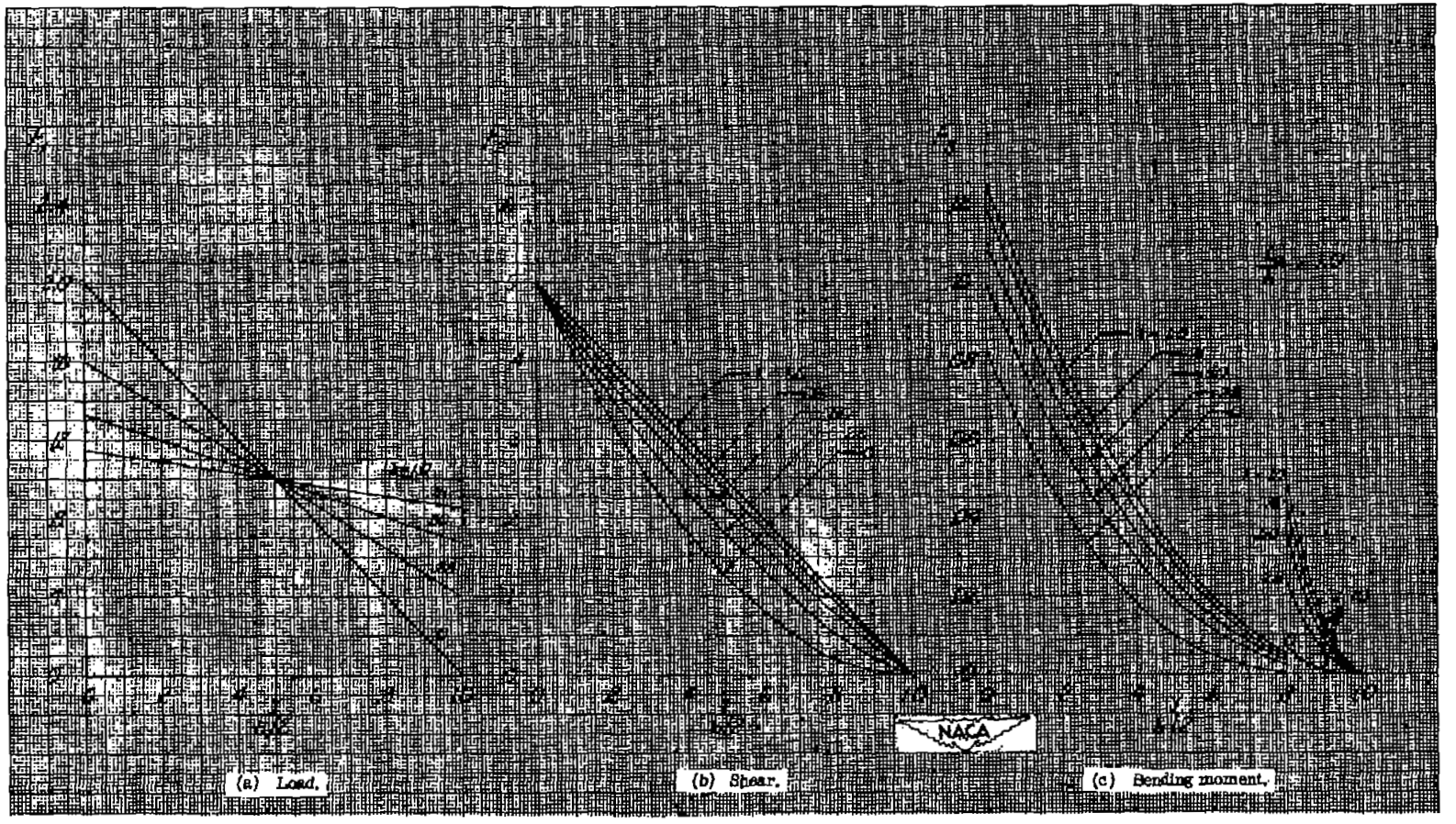

Figure 4.- Distributions due to additional air load, ailerons-deflected air load, and wing weight and normal inertia.

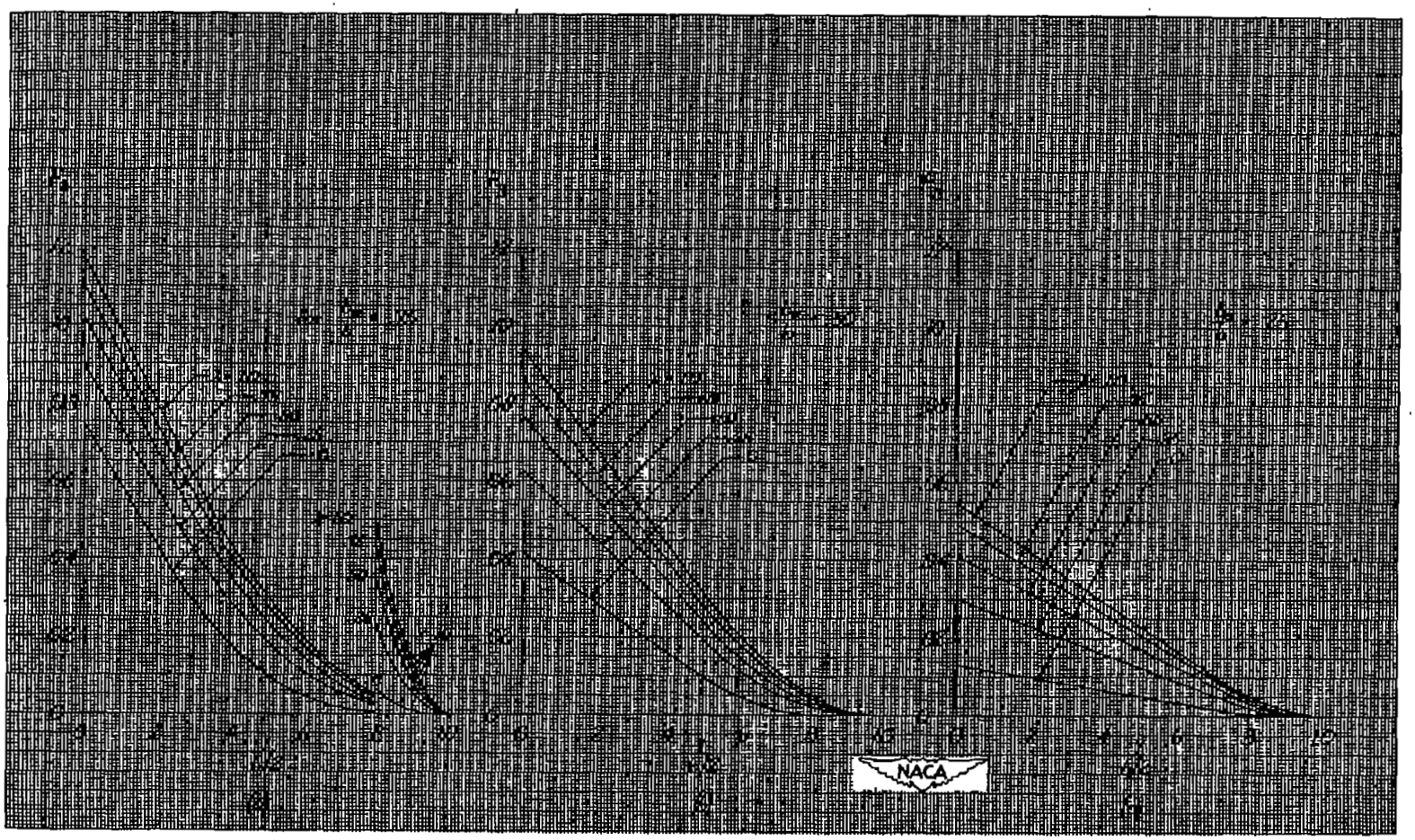

Figure 5.- Bending-moment distributions due to ailerons-deflected load for several aileron spans.

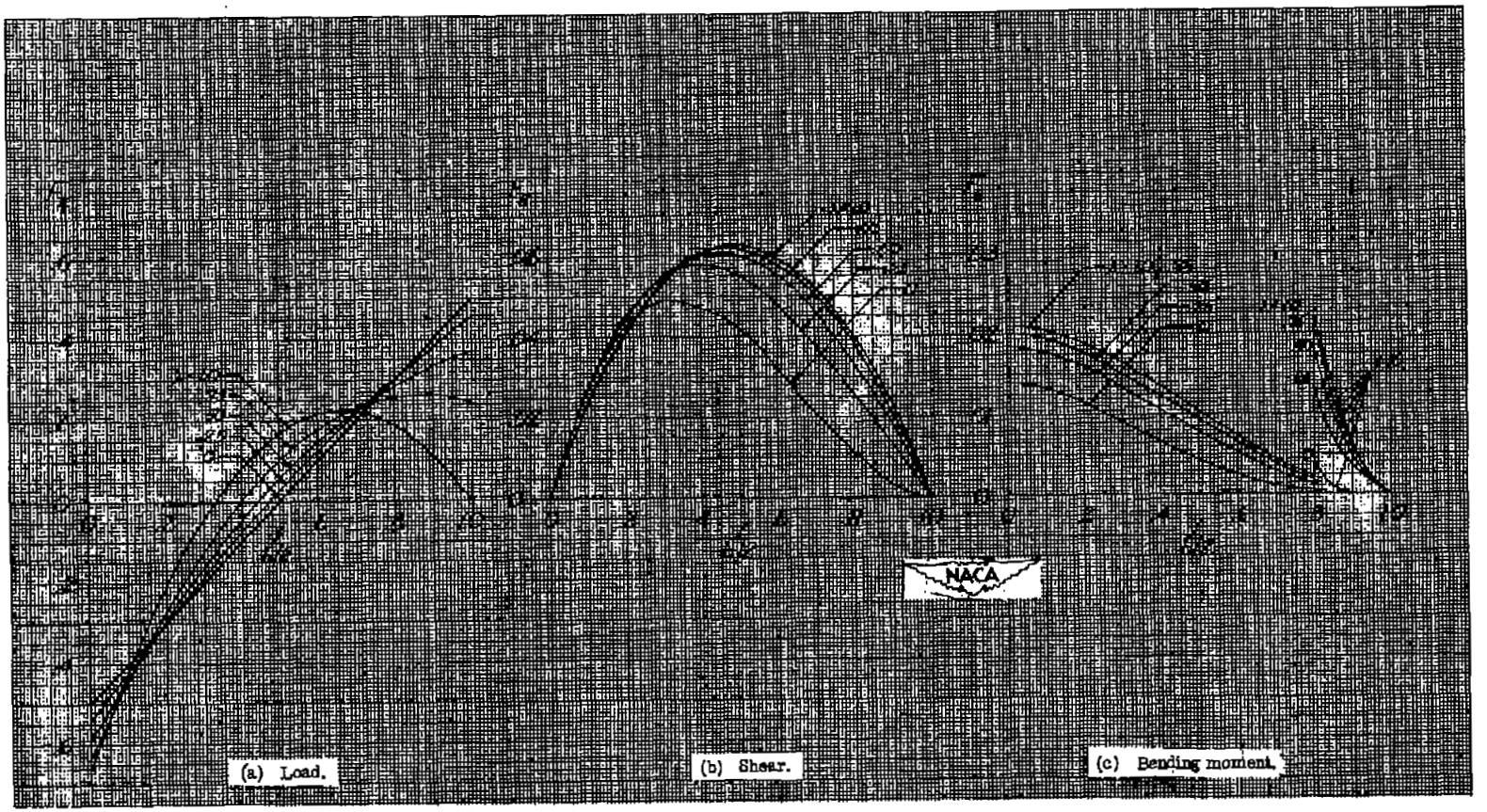

Figure 6.- Distributions due to linear built-in twist.

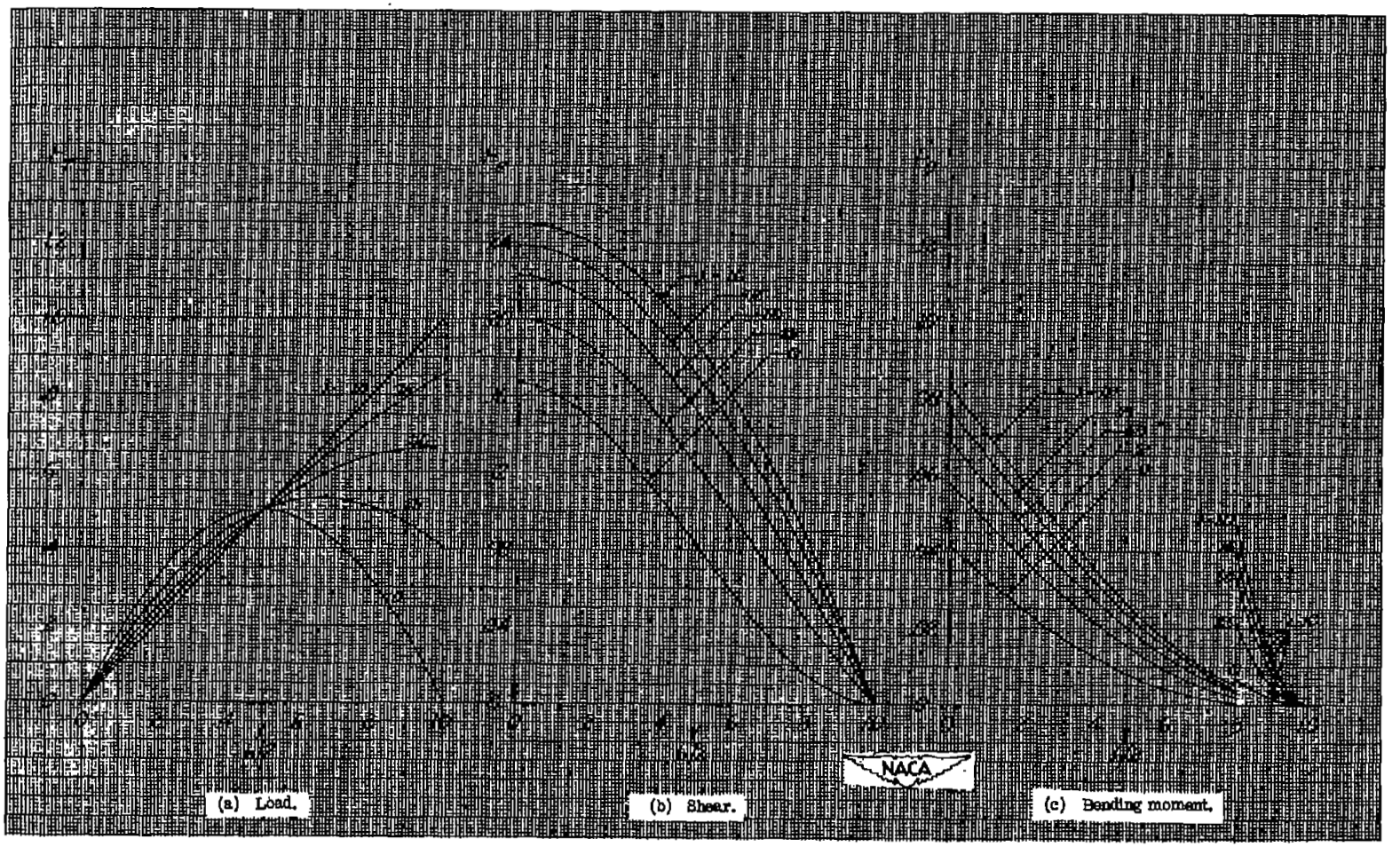

Figure 7.- Distributions due to damping in roll and angular inertia loads.

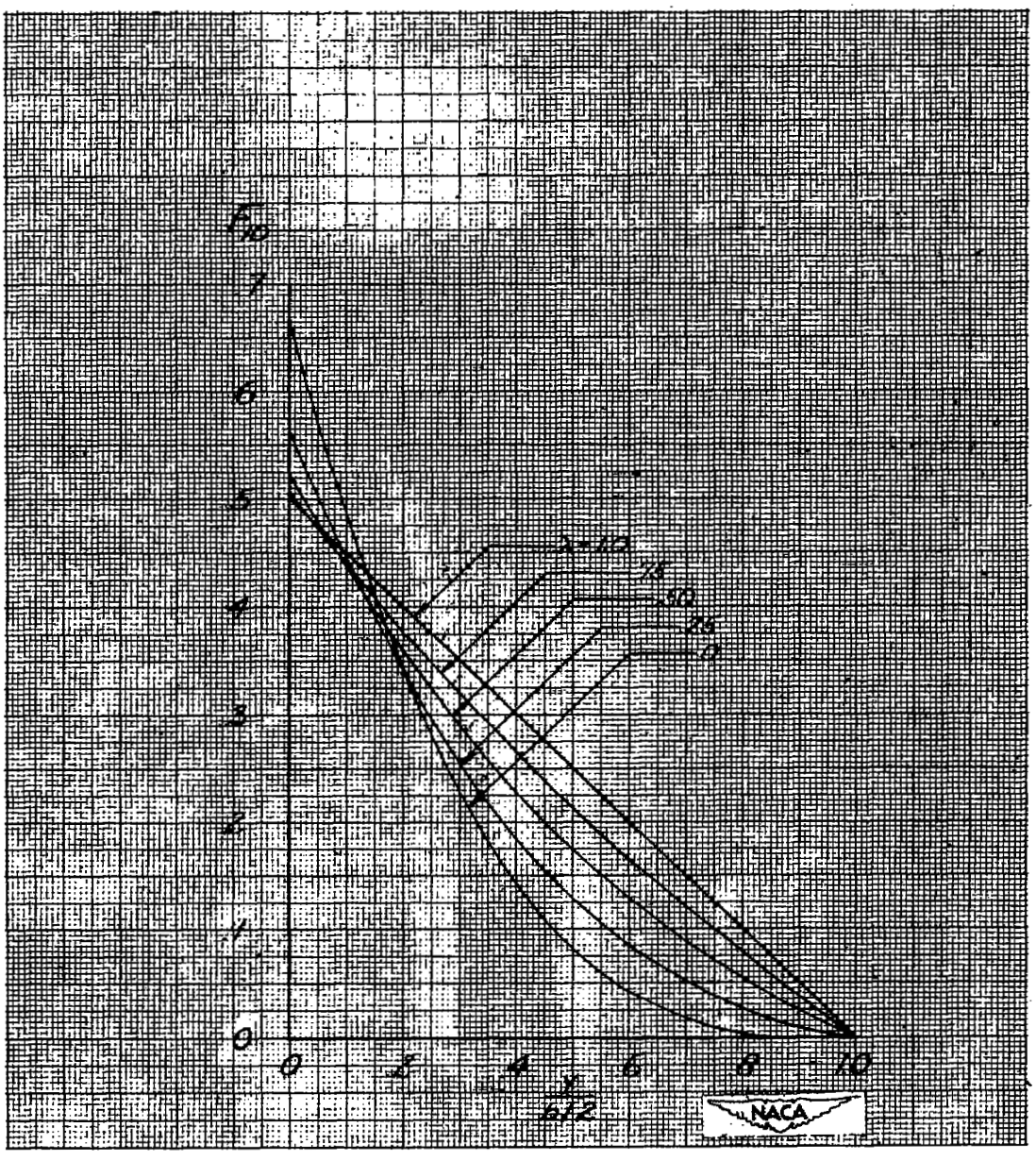

Figure 8.- Accumulated torque due to section pitching moments.

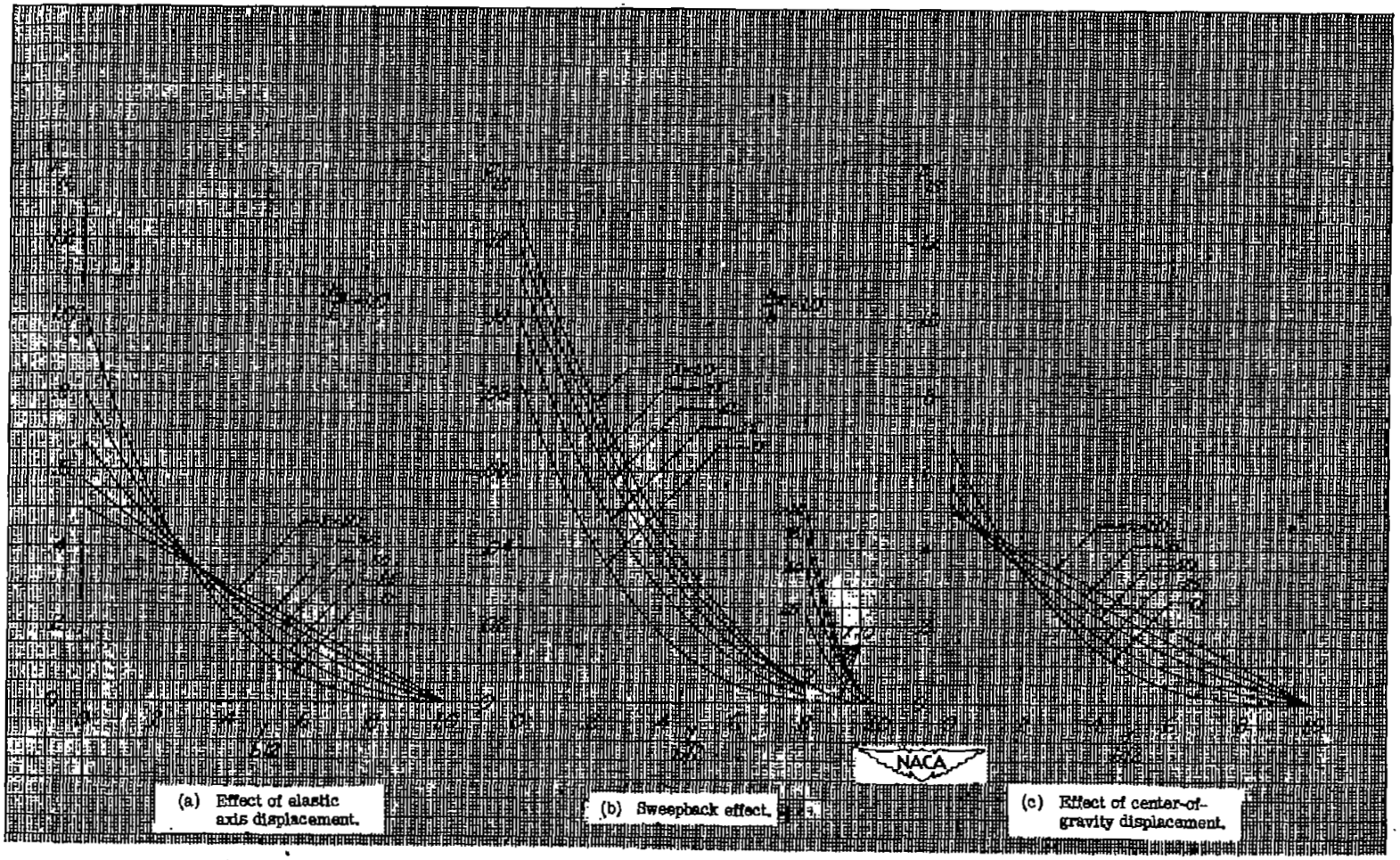

Figure 9.- Accumulated torque distributions for additional air load, ailerons-deflected air load, and wing weight and normal inertia.

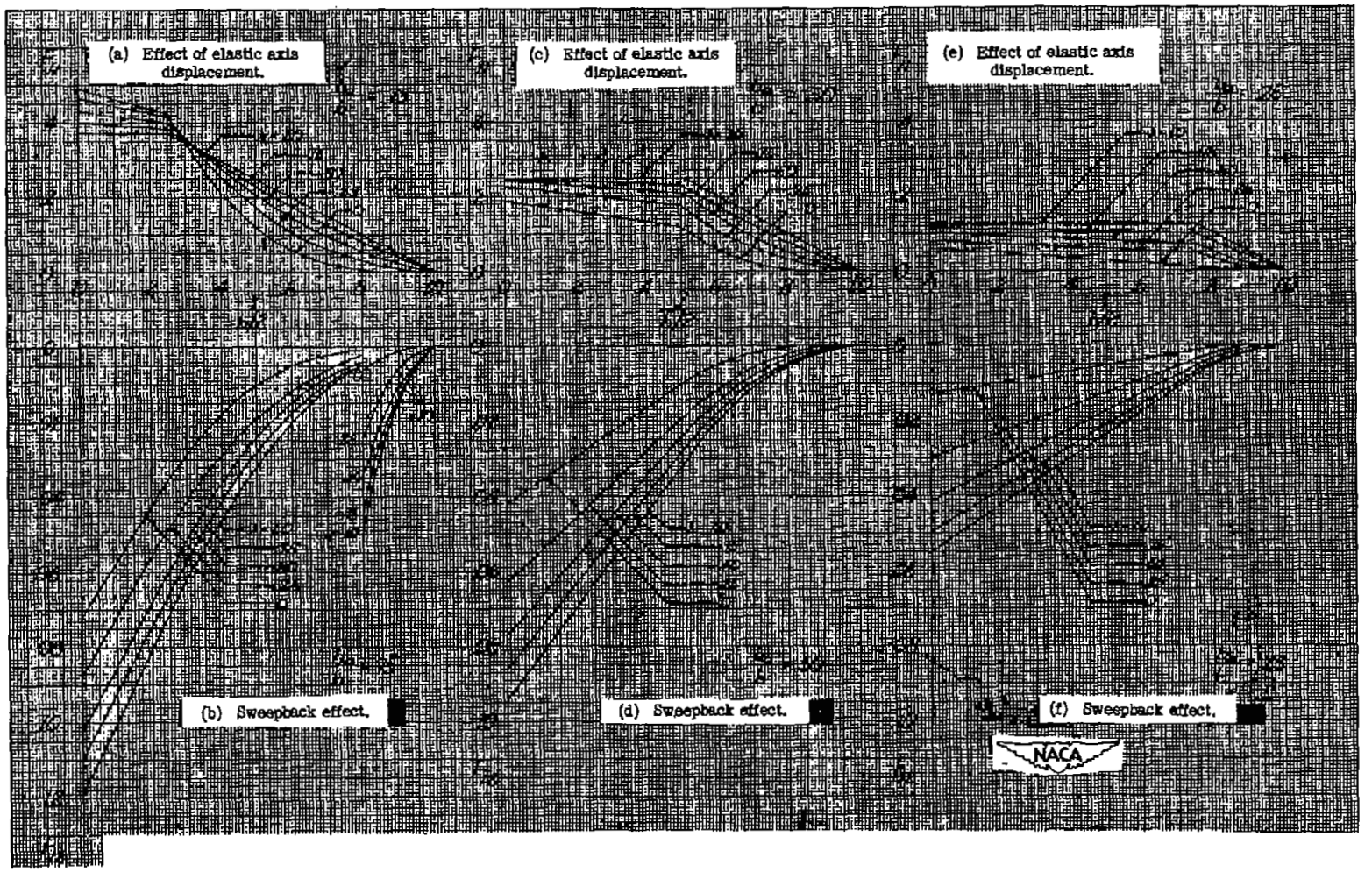

Figure 10.- Accumulated torque distributions due to ailerons-deflected load for several aileron spans.

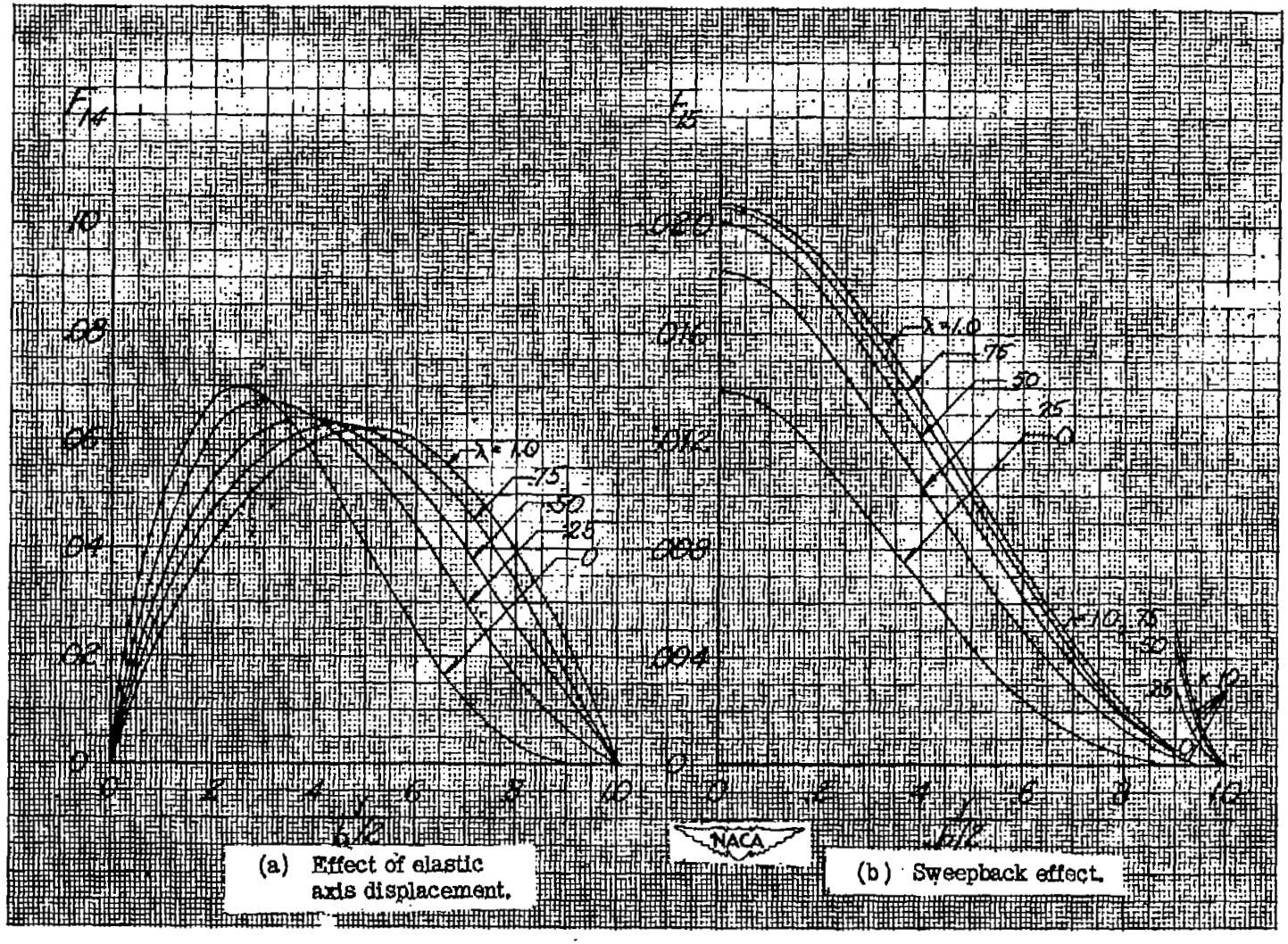

Figure 11.- Accumulated torque distribution due to built-in twist load.

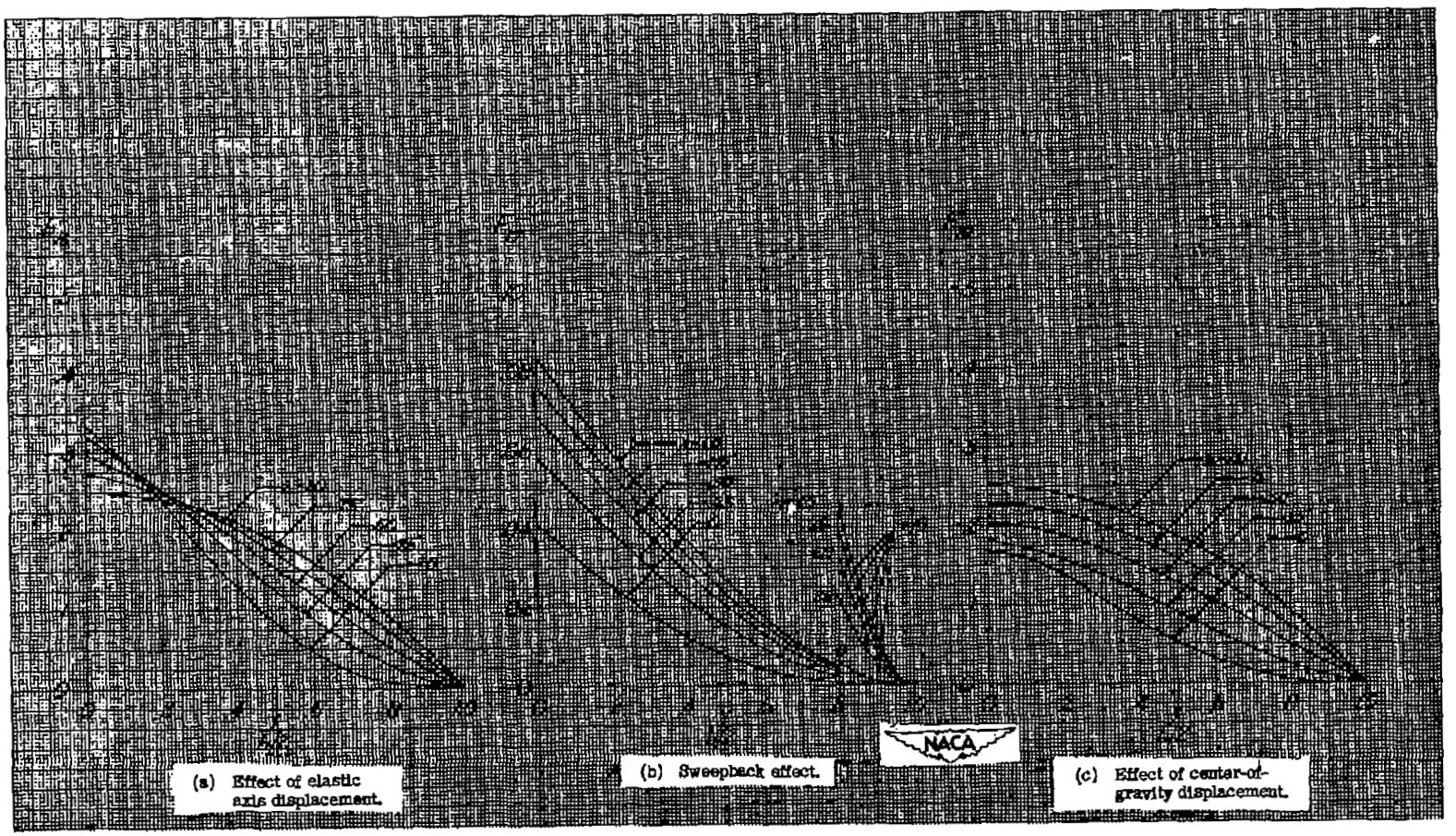

Figure 12.- Accumulated torque distributions due to damping in roll and angular inertia loads.

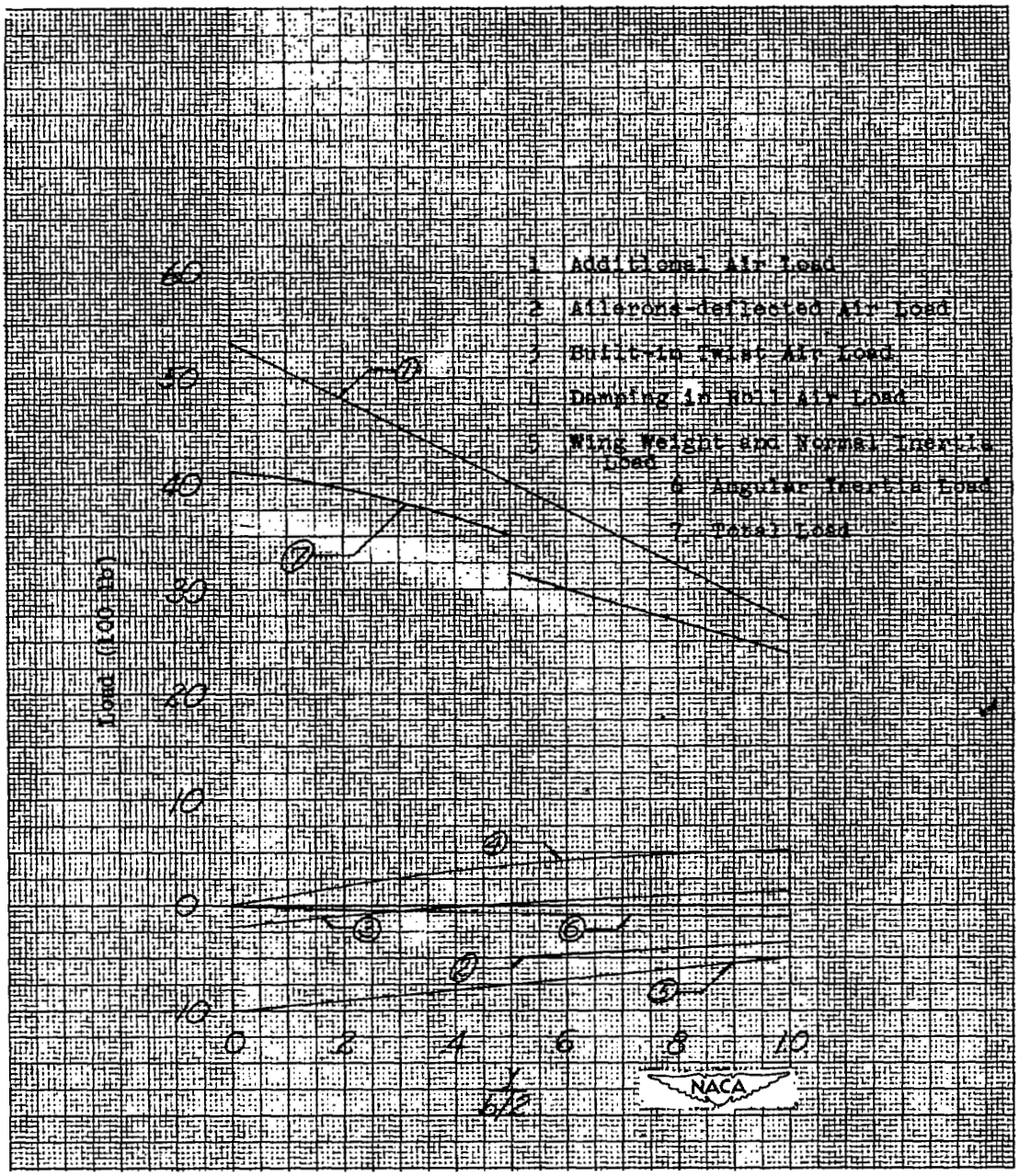

Figure 13.- Results of typical example showing components of total load distribution.

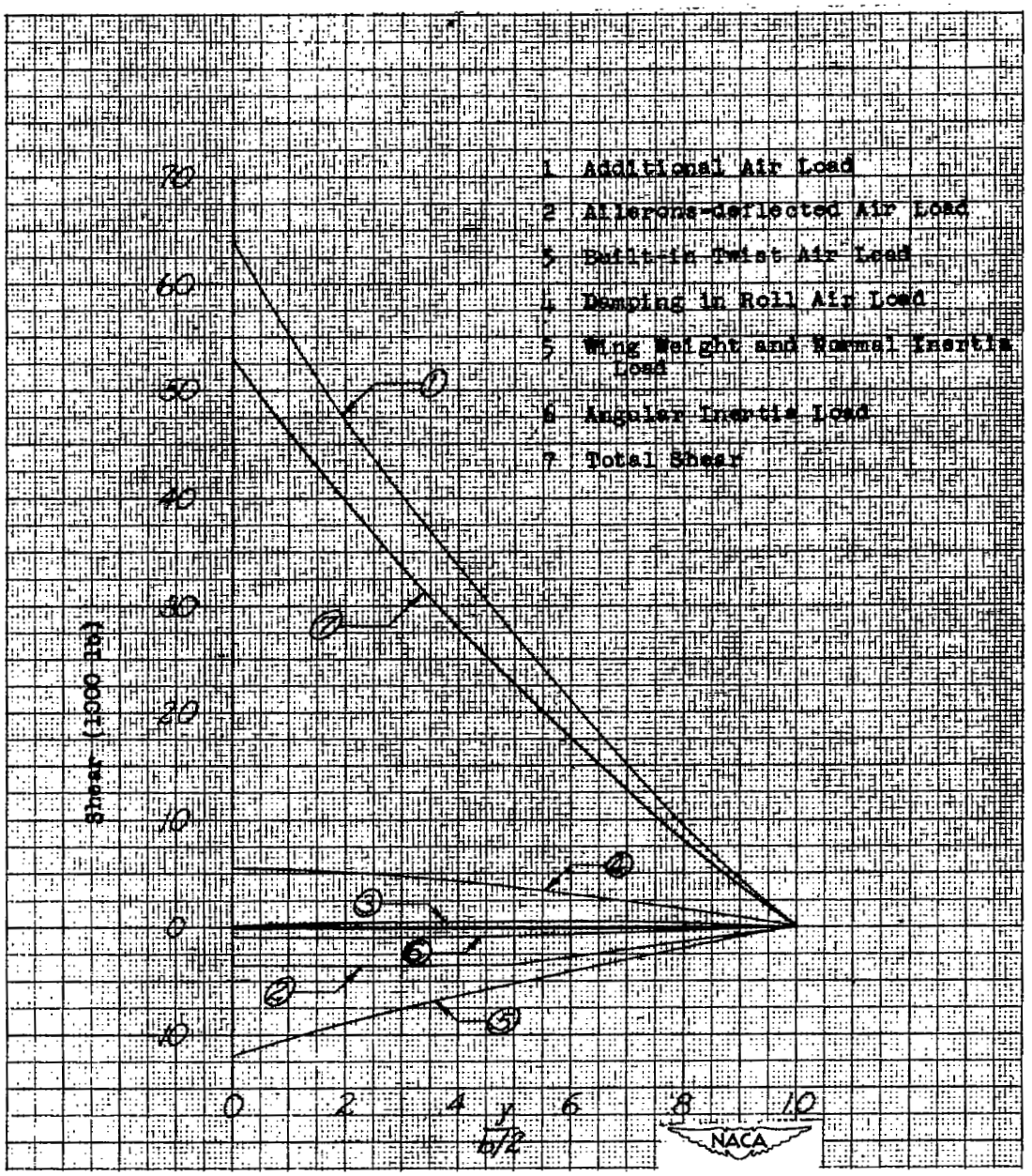

Figure 14.- Results of typical example showing components of total shear distribution.

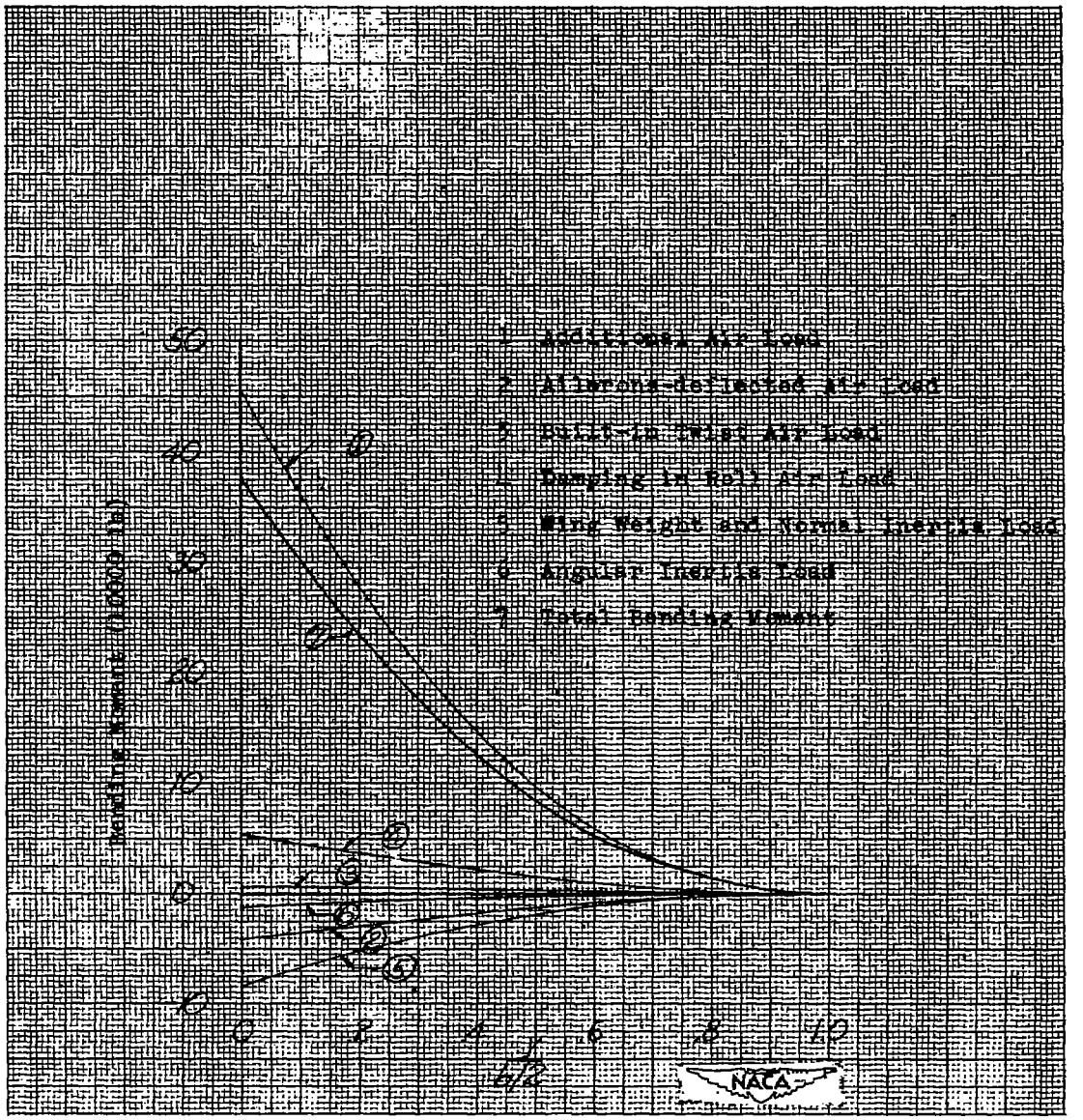

Figure 15.- Results of typical example showing components of total bending-moment distribution.

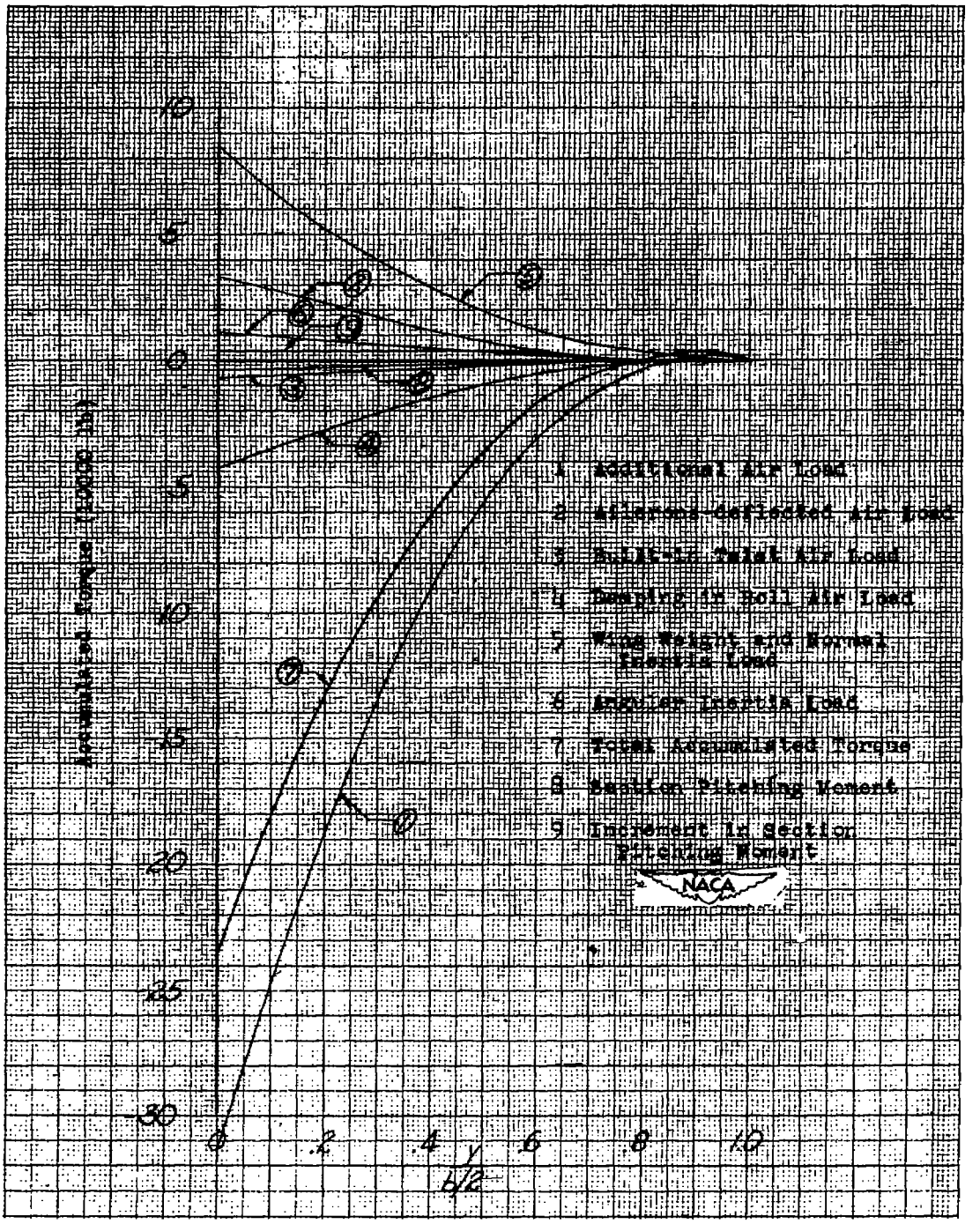

Figure 16.- Results of typical example showing components of total accumulated torque distribution.

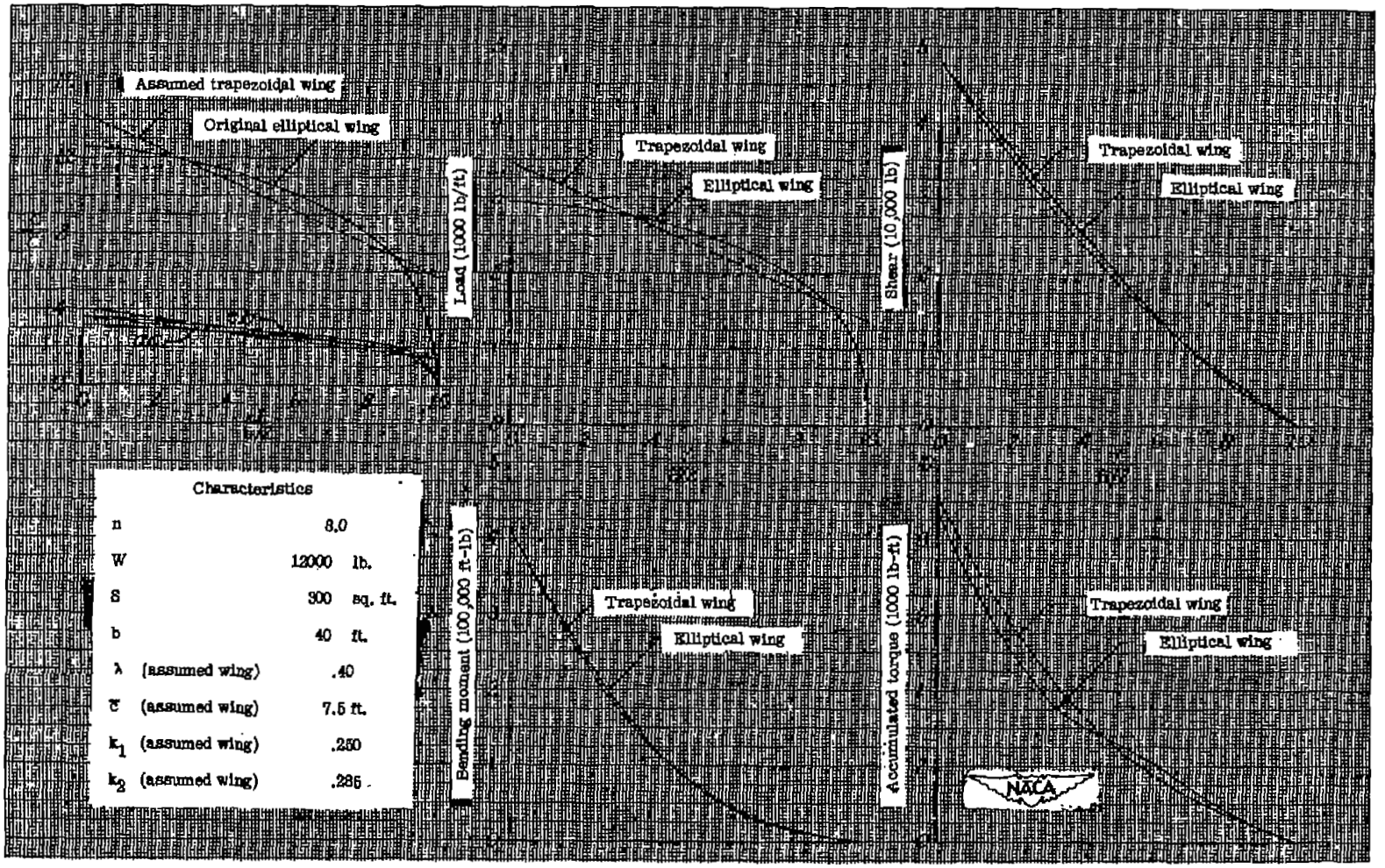

Figure 17.- Results, with respect to the additional air load, from use of the charts with wing of plan form other than trapezoidal.

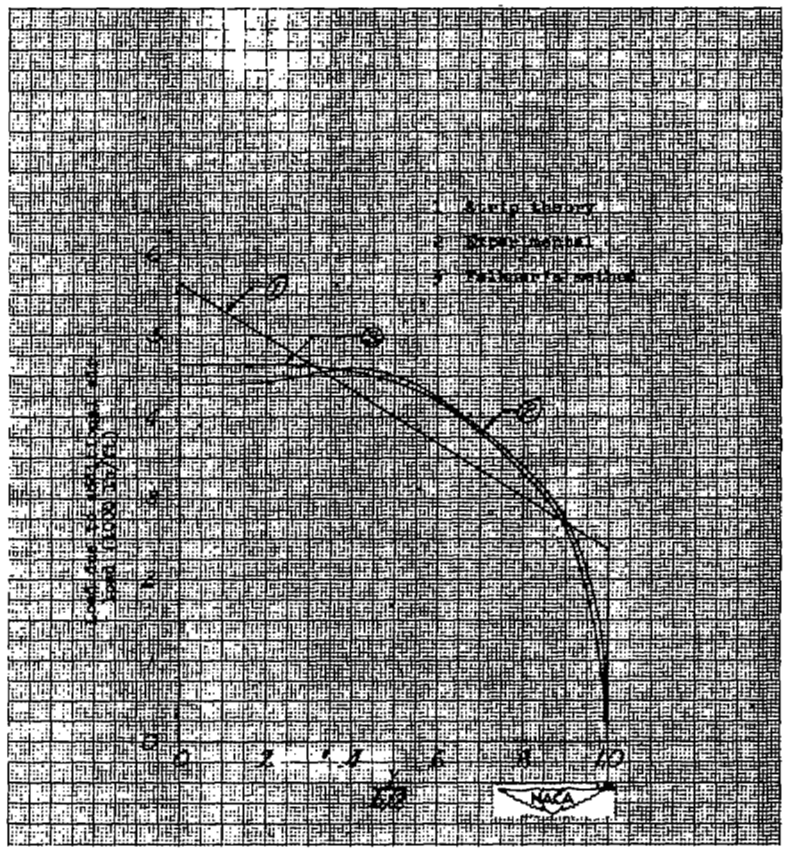

Figure 18.- A comparison of spanwise loads obtained for theoretical airplane of example with $\lambda = 0.418$ at subsonic speeds.

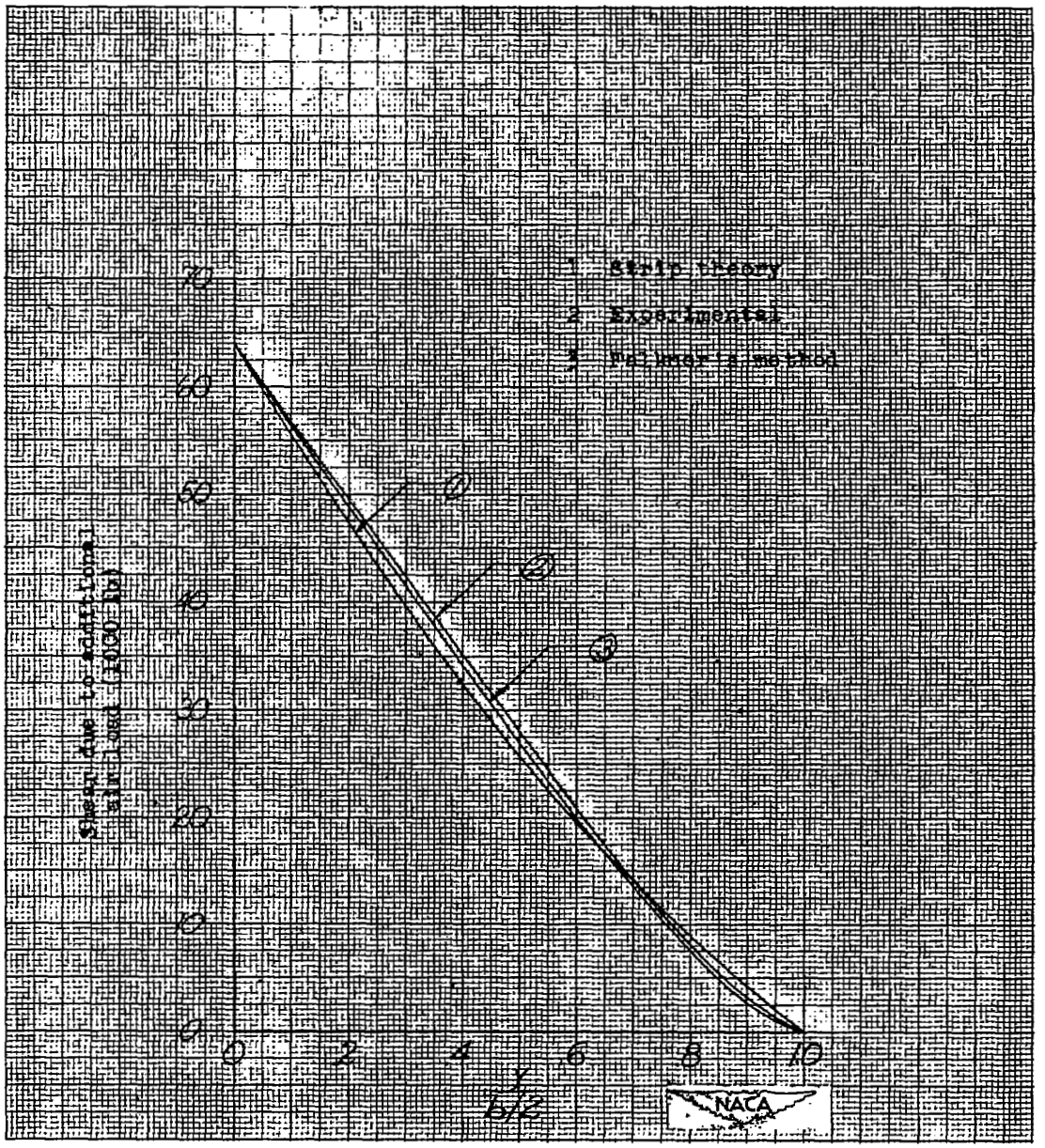

Figure 19.- . A comparison of spanwise shears obtained for theoretical airplane of example with $\lambda = 0.418$ at subsonic speeds.

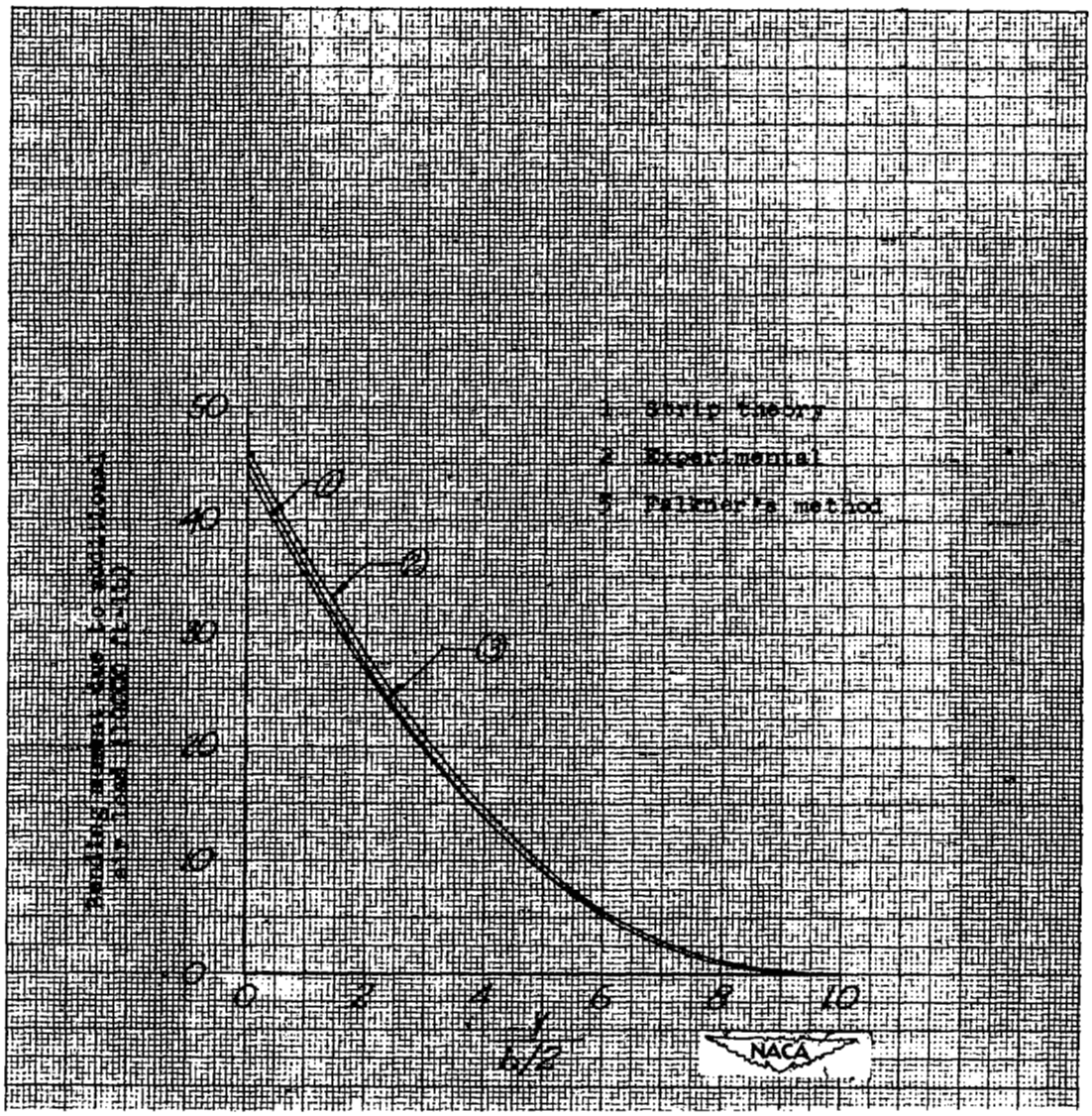

Figure 20.- A comparison of spanwise bending moments obtained fo theoretical airplane of example with $\lambda = 0.418$ at subsonic speeds.

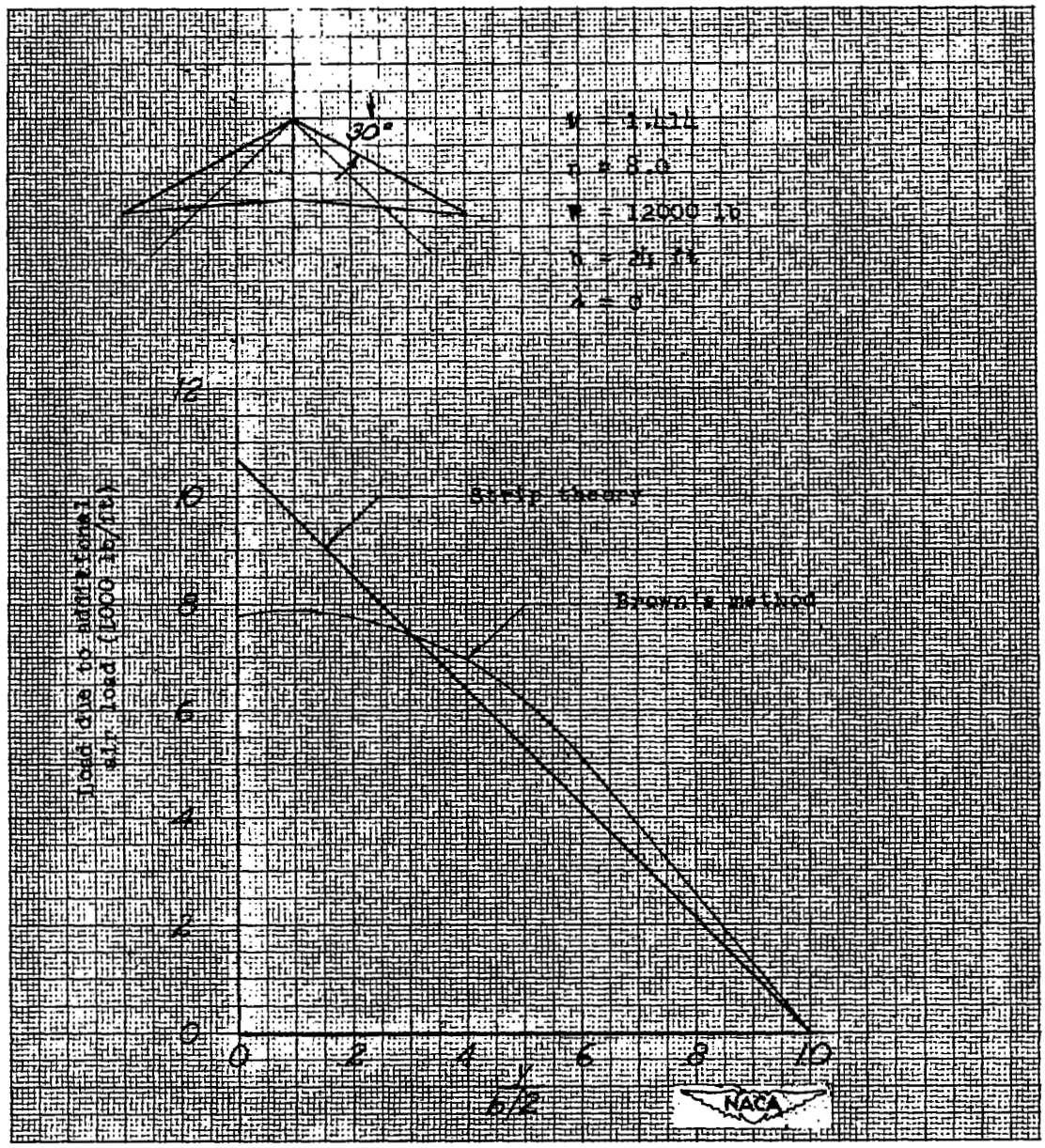

Figure 21.- A comparison of spanwise loads obtained at supersonic speed for wing shown.

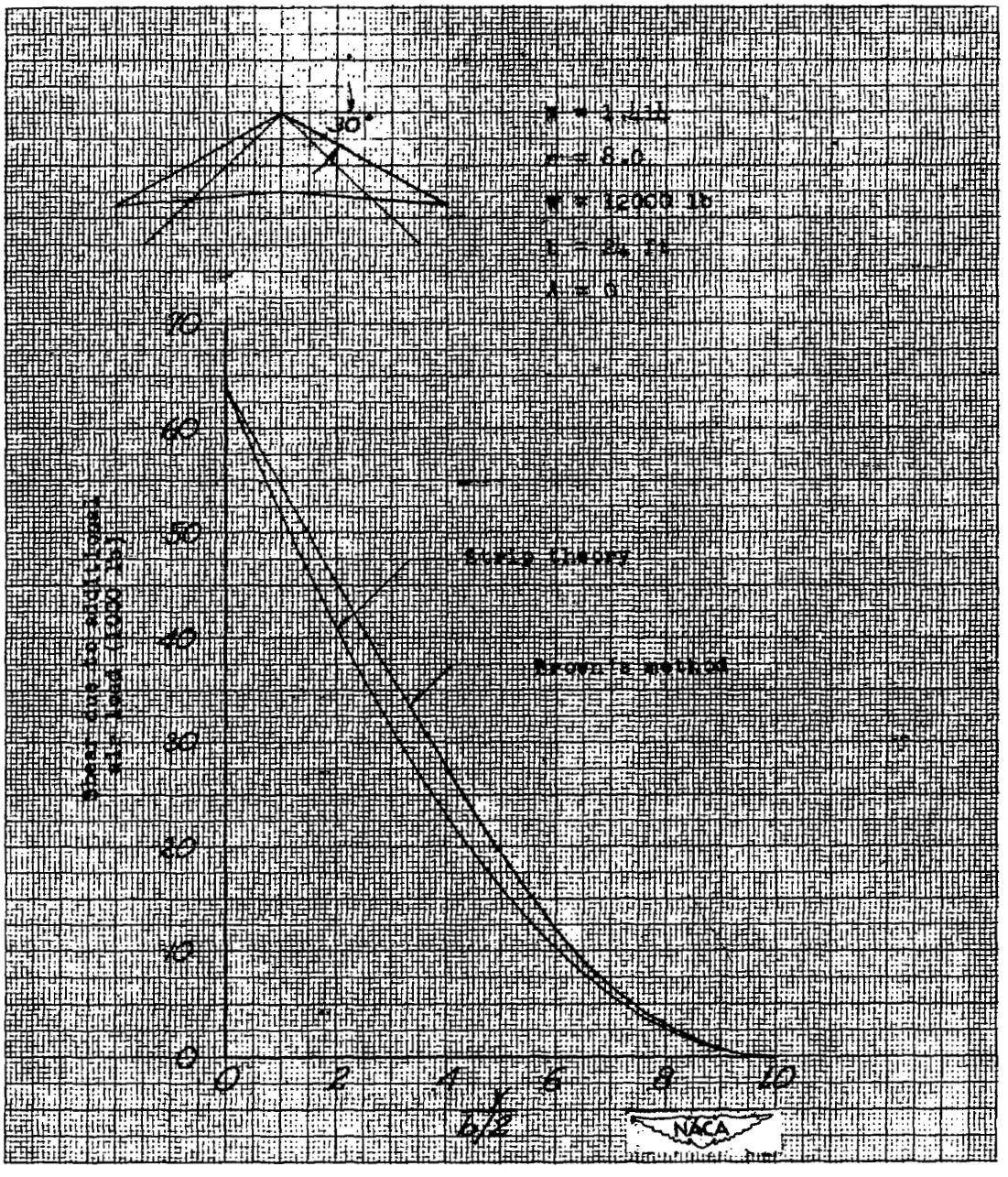

Figure 22.- A comparison of spanwise shears obtained at supersonic speed for wing shown.

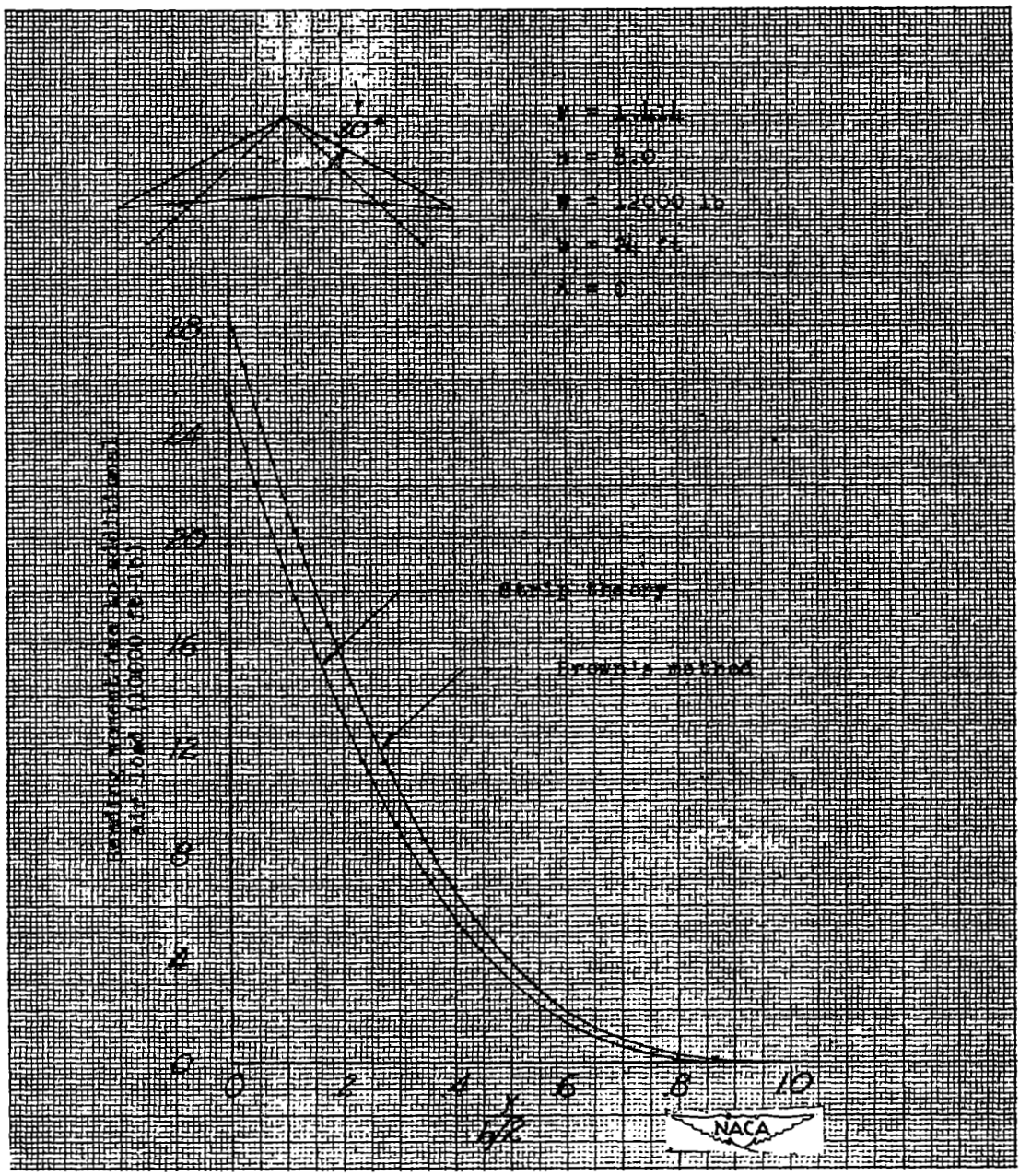

Figure 23.- A comparison of spanwise bending moments obtained at supersonic speed for wing shown.